Optimal spatial patterns in feeding, fishing, and pollution

Hannes Uecker, Institut für Mathematik, Carl von Ossietzky Universität Oldenburg
hannes.uecker@uol.de, March 1, 2021

Abstract

Infinite time horizon spatially distributed optimal control problems may show so–called optimal diffusion induced instabilities, which may lead to patterned optimal steady states, although the problem itself is completely homogeneous. Here we show that this can be considered as a generic phenomenon, in problems with scalar distributed states, by computing optimal spatial patterns and their canonical paths in three examples: optimal feeding, optimal fishing, and optimal pollution. The (numerical) analysis uses the continuation and bifurcation package `pde2path` to first compute bifurcation diagrams of canonical steady states, and then time–dependent optimal controls to control the systems from some initial states to a target steady state as $t \to \infty$. We consider two setups: The case of discrete patches in space, which allows to gain intuition and to compute domains of attraction of canonical steady states, and the spatially continuous (PDE) case.

1 Introduction

Infinite time horizon optimal control (OC) problems with ODE constraints deal with maximizing discounted time integrals

$$V(v_0) := \max_{q(\cdot)\in\mathcal{Q}} J(v_0, q(\cdot)), \quad J(v_0, q(\cdot)) := \int_0^\infty \mathrm{e}^{-\rho t} J_c(v(t), q(t))\,\mathrm{d}t, \tag{1.1a}$$

where $J_c : \mathbb{R}^n \times \mathbb{R}^{n_q} \to \mathbb{R}$ is a given objective function, $v = v(t) \in \mathbb{R}^n$ are the states of a system, $q \in \mathcal{Q} \subset L^\infty([0,\infty), \mathbb{R}^{n_q})$ is a control, $\rho > 0$ is a discount rate, and the states fulfill the initial value problem

$$\frac{\mathrm{d}}{\mathrm{d}t} v = f(v, q), \quad v|_{t=0} = v_0. \tag{1.1b}$$

The max in (1.1a) runs over all *admissible* controls q, which will be specified below, and the discounted time integral in (1.1a) is typical for economic problems, where "profits now" weight more than mid or far future profits. See, e.g., [FH86, LW07, GCF+08] for a multitude of examples from various settings, including classical economics, bioeconomics, and drug and terror control.

A major tool for (1.1) is Pontryagin's Maximum Principle [PBGM62], which first has been used for finite time horizon OC problems, where the integral in (1.1a) runs to some finite T, and where there may be a scrap value at T added to the integral. For the infinite horizon problem, the setting is as follows: Assume that an optimal control $q^* \in \mathcal{Q}$ exists, and introduce the co-states (or shadow prices, or Lagrange multipliers) $\lambda = \lambda(t) \in \mathbb{R}^n$, and the Hamiltonian (density)

$$H = H(v, \lambda, q) = J_c(v, q) + \lambda^T f(v, q),$$

where v, λ and f are column vectors and hence $\lambda^T f$ is the standard $\mathbb{R}^n$ inner product of λ and f. Under some technical asumptions, namely that optimal solutions are sufficiently smooth and fulfill the limiting inter-temporal transversality condition

$$\lim_{t\to\infty} \mathrm{e}^{-\rho t}\lambda^T(t)v(t) = 0, \tag{1.2}$$

we obtain that at each time $t > 0$, necessarily

$$q^*(t) = \operatorname*{argmax}_q H(v(t), \lambda(t), q), \tag{1.3a}$$

which we assume can be solved uniquely for $q = q(v, \lambda)$, and that (v, λ) must fulfill the so–called *canonical system*

$$\frac{\mathrm{d}}{\mathrm{d}t}v = \partial_\lambda \widetilde{H}(v, \lambda) = f(v, q), \quad v|_{t=0} = v_0, \tag{1.3b}$$

$$\frac{\mathrm{d}}{\mathrm{d}t}\lambda = \rho\lambda - \partial_v \widetilde{H}(v, \lambda) = (\rho - \partial_v f^T(v, q))\lambda, \tag{1.3c}$$

where $\widetilde{H}(v, \lambda) = H(v, \lambda, q(v, \lambda))$ is the maximized Hamiltonian. See [GCF+08, §3.7, §3.8], and [Tau15] for precise statements of Pontryagin's Maximum Principle yielding the necessary first order optimality conditions (1.3), for (concavity) assumptions yielding sufficiency of (1.3), and a guide to the vast literature. See also App.A for a formal derivation of (1.3) using classical calculus of variations, in an extension to OC problems with PDE constraints, which are discussed below.

Problems similar to (1.1) can also be studied in a spatial setting, in at least two different ways. First, we may assume that the states are defined at $n_p \in \mathbb{N}$ discrete patches (or sites), coupled by discrete diffusion. For simplicity here using $n_p = 2$ and assuming scalar states and controls at each patch, we thus have states $v(t) = (v_1(t), v_2(t)) \in \mathbb{R}^2$ and controls $q(t) = (q_1(t), q_2(t)) \in \mathbb{R}^2$, and consider

$$V(v(0)) := \max_{q(\cdot)} J(v(0), q(\cdot)), \quad J(v(0), q(\cdot)) = \int_0^\infty \mathrm{e}^{-\rho t} J_{c,a}(v(t), q(t))\,\mathrm{d}t, \tag{1.4a}$$

where $J_{c,a}(v, c) = \frac{1}{2}(J_c(v_1, q_1) + J_c(v_2, q_2))$ is the averaged objective, subject to

$$\frac{\mathrm{d}}{\mathrm{d}t}v_1 = f_{\mathrm{loc}}(v_1, q_1) + D(v_2 - v_1), \qquad \frac{\mathrm{d}}{\mathrm{d}t}v_2 = f_{\mathrm{loc}}(v_2, q_2) + D(v_1 - v_2), \tag{1.4b}$$

with diffusion coefficient $D > 0$, and where f_{loc} denotes the local right hand side. We call this a *two-patch problem* (2P problem), in contrast to the *single patch problem* (1P problem) (1.1). Pontryagin's Maximum Principle with the Hamiltonian

$$H(v, \lambda, q) = J_c(v, q) + \lambda^T \left(f(v, q) + D \begin{pmatrix} v_2 - v_1 \\ v_1 - v_2 \end{pmatrix} \right), \tag{1.5}$$

f=$(f_{\mathrm{loc}}(v_1, q_1), f_{\mathrm{loc}}(v_2, q_2))$, costate vector λ=$(\lambda_1, \lambda_2)^T$, and limiting transversality condition

$\lim_{t\to\infty} \mathrm{e}^{-\rho t}\lambda(t)^T v(t)=0$ yields $q_i = q_i(v_i, \lambda_i)$, and the 4–component canonical system

$$\frac{\mathrm{d}}{\mathrm{d}t}v = f(v,q) + D\begin{pmatrix} v_2-v_1 \\ v_1-v_2 \end{pmatrix}, \quad v|_{t=0} = v_0, \tag{1.6a}$$

$$\frac{\mathrm{d}}{\mathrm{d}t}\lambda = (\rho - \partial_v f(v,q)^T)\lambda - D\begin{pmatrix} \lambda_2-\lambda_1 \\ \lambda_1-\lambda_2 \end{pmatrix}. \tag{1.6b}$$

Second, instead of discrete patches we may assume continuous space $x \in \Omega \subset \mathbb{R}^d$, and that the states $v : \Omega \times [0,\infty) \to \mathbb{R}^N$ and the control $q : \Omega \times [0,\infty) \to \mathbb{R}$ are functions of x and t, and consider objectives of the form

$$V(v_0) := \max_{q(\cdot,\cdot)} J(v_0, q(\cdot,\cdot)), \qquad J(v_0,q) := \int_0^\infty \mathrm{e}^{-\rho t} J_{ca}(v(\cdot,t), q(\cdot,t))\,\mathrm{d}t, \tag{1.7a}$$

with $J_{ca}(v(\cdot,t), q(\cdot,t)) = \langle J_c(v(x,t), q(x,t))\rangle$, where, to make results over different domains easily comparable,

$$\langle h\rangle := \frac{1}{|\Omega|}\int_\Omega h(x)\,\mathrm{d}x \tag{1.7b}$$

is the spatial average of $h : \Omega \to \mathbb{R}$. The states fulfill the PDE initial value problem

$$\partial_t v = f(v,q) + D\Delta v, \quad v|_{t=0} = v_0, \tag{1.7c}$$

together with some boundary conditions (BCs), which for simplicity we take as homogeneous Neumann (aka zero–flux) BCs

$$\partial_n v = 0. \tag{1.7d}$$

In (1.7c), $D \in \mathbb{R}^{N\times N}$ is a positive (semi–) definite diffusion matrix, and $\Delta = \partial_{x_1}^2 + \ldots + \partial_{x_d}^2$ is the Laplacian. Formally[1], we may then proceed as above and define the Hamiltonian

$$H(v,\lambda,q) = J_{ca}(t) + \langle \lambda(\cdot,t)^T (f(v(\cdot,t), q(\cdot,t)) + D\Delta v(\cdot,t))\rangle, \tag{1.8}$$

and require the limiting transversality condition

$$\lim_{t\to\infty} \mathrm{e}^{-\rho t}\langle \lambda(\cdot,t)^T v(\cdot,t)\rangle = 0, \tag{1.9}$$

leading to canonical systems of the form

$$\partial_t v = \partial_\lambda \widetilde{H}(v,\lambda) = f(v,q) + D\Delta v, \quad v|_{t=0} = v_0, \tag{1.10a}$$

$$\partial_t \lambda = \rho\lambda - \partial_v \widetilde{H}(v,\lambda) = (\rho - \partial_v f(v,q)^T)\lambda - D\Delta\lambda, \tag{1.10b}$$

with Neumann BCs for v and λ, and where $\widetilde{H}$ denotes the pointwise maximized Hamiltonian

$$\widetilde{H} = \widetilde{H}(v(x,t), \lambda(x,t)) = H(v(x,t), \lambda(x,t), q(v(x,t), \lambda(x,t))). \tag{1.11}$$

[1] see Appendix A

1.1 A solution method

In the canonical systems (1.3), (1.6) and (1.10), we only have initial conditions $v|_{t=0} = v_0$ for the states, while the costates (and hence the control) at $t = 0$ are free. Moreover, for instance in (1.10b) we have "backward diffusion" such that (1.10) would be ill–posed as an initial value problem. Nevertheless, roughly speaking we have reduced the choice of q in (1.7a) to the choice of $\lambda_0 = \lambda|_{t=0}$ in (1.10), and similarly for (1.1) and (1.4). One way to proceed is to first compute steady states $(\hat{v}, \hat{\lambda}) \in \mathbb{R}^{2n}$ of (1.3), resp. (1.6) or (1.10). Here we first assume the ODE case, and below comment on the PDE case with $n = Nn_p$ after spatial discretization, with n_p the number of discretization points.

A steady state $(\hat{v}, \hat{\lambda})$ of the canonical system is called a *canonical steady state* (CSS)[2] , while a time dependent solution is called a *canonical path*. For notational convenience[3] we set $u = (v, \lambda) \in \mathbb{R}^{2n}$ and write the canonical system in the condensed form

$$\frac{\mathrm{d}}{\mathrm{d}t}u = -G(u), \quad v|_{t=0} = v_0 \in \mathbb{R}^n. \tag{1.12}$$

After computing CSSs $\hat{u} = (\hat{v}, \hat{\lambda})$, together with their value $J(\hat{u}) = J_c(\hat{u})/\rho$, we aim to find canonical paths $u : [0, \infty) \to \mathbb{R}^{2n}$ with $\lim_{t\to\infty} u(t) = \hat{u}$ for some CSS $\hat{u} = (\hat{v}, \hat{\lambda})$. For this, the initial states $v_0 \in \mathbb{R}^n$ must lie in the stable manifold $W_s(\hat{u})$ of $\hat{u}$. Therefore, for generic v_0 near $\hat{v}$, a necessary and sufficient condition for such a canonical path to $\hat{u}$ to exist is that $\dim W_s(\hat{u}) \geq n$. On the other hand, from the structure of (1.3) it follows that $\dim W_s(\hat{u}) \leq n$, see, e.g., [GU17]. A CSS $\hat{u}$ with $\dim W_s(\hat{u}) = n$ is said to have the *saddle point property* (SPP), which can be seen as a local stability, because if $\dim W_s(\hat{u}) = n$ then there generically exists a canonical path to $\hat{u}$ from nearby initial states v_0. We call $d(\hat{u}) := n - \dim W_s(\hat{u})$ the *defect of the CSS* $\hat{u}$, such that the SPP corresponds to $d(\hat{u}) = 0$.

Importantly, the nonlinear canonical systems of type (1.12) typically come with a number of parameters, e.g., the discount rate ρ, and thus a useful strategy is to search for CSSs in a continuation and bifurcation setting. This quickly becomes difficult or impossible analytically, and hence some numerics are useful. In particular, except for rare exceptional (basically linear) cases, for the computation of canonical paths numerics are required. This typically proceeds by a continuation procedure in the initial states in the form $\widetilde{v}_0 = \alpha v_0 + (1-\alpha)\hat{v}$, starting with small α and initial guess $u(t) \equiv \hat{u}$ for the canonical path. Using the last canonical path as an initial guess for $\alpha + \delta$, we may increase α, and if we can reach $\alpha = 1$, then we have found the desired canonical path u from v_0 to $\hat{u}$. In this case we say that v_0 is in the *domain of attraction* $\mathcal{A}(\hat{u})$ of $\hat{u}$, i.e.,

$$\mathcal{A}(\hat{u}) := \{v_0 \in \mathbb{R}^n : \text{there exists, by choice of } \lambda_0 \in \mathbb{R}^n, \text{ a canonical path from } v_0 \text{ to } \hat{u}\}. \tag{1.13}$$

Numerically, the convergence $\lim_{t\to\infty} u(t) = \hat{u}$ is approximated by choosing a truncation time t_0 and requiring that

$$\|u(t_0) - \hat{u}\| < \varepsilon \text{ (in some norm), and } u(t_0) \in E_s(\hat{u}) \text{ (the stable eigenspace)}, \tag{1.14}$$

as $E_s(\hat{u})$ close to $\hat{u}$ approximates $W_s(\hat{u})$. Setting $u{=}\hat{u}{+}w$ yields the linearization $\frac{\mathrm{d}}{\mathrm{d}t}w{=}-\partial_u G(\hat{u})w$, and the decay of w to 0 is determined by the smallest positive (due to the convention $\frac{\mathrm{d}}{\mathrm{d}t}u = -G(u)$

[2]the symbol $\hat{}$ is custom for a CSS and has nothing to do with Fourier transform

[3]here we deviate from standard notation in OC, where u often is the symbol for the control

in (1.12)) eigenvalue μ_1 of $\partial_u G(\hat{u})$. Thus, $\mathrm{e}^{-\mu_1 t} = \varepsilon$ yields an estimate

$$t_0 = (-\ln \varepsilon)/\mu_1 \tag{1.15}$$

for the truncation time t_0 in (1.14), which for small μ_1 can be quite large.

All of the above applies equally to 1P and 2P problems. Moreover, any CSS $\hat{u}$ of the 1P problem yields a CSS $(\hat{v}, \hat{v}, \hat{\lambda}, \hat{\lambda})$ (two identical copies) of the 2P problem, which hence we call a spatially homogeneous or *flat* CSS (FCSS), and the same holds for canonical paths. Additionally, the 2P problem may have inhomogeneous CSSs $(\hat{v}_1, \hat{v}_2, \hat{\lambda}_1, \hat{\lambda}_2)$ with $\hat{v}_1 \neq \hat{v}_2$ (and then typically also $\hat{\lambda}_1 \neq \hat{\lambda}_2$), which we call *patterned* CSSs (PCSSs).[4] If (at some fixed parameter values) several CSS $\hat{u}$ with $d(\hat{u}) = 0$ exist, then from a given initial state v_0 we can try to compute canonical paths to each of them, and compare their values, which we approximate as

$$J = \int_0^\infty \mathrm{e}^{-\rho t} J_c(t)\,\mathrm{d}t = \int_0^{t_0} \mathrm{e}^{-\rho t} J_c(t)\,\mathrm{d}t + \int_{t_0}^\infty \mathrm{e}^{-\rho t} J_c(t)\,\mathrm{d}t \approx \int_0^{t_0} \mathrm{e}^{-\rho t} J_c(t)\,\mathrm{d}t + \frac{\mathrm{e}^{-\rho t_0}}{\rho} J_c(t_0). \tag{1.16}$$

The canonical path with the lower J is then clearly suboptimal, while the one with the higher J might be optimal.

The continuation in the initial states is implemented in `pde2path`, with PDEs (PDE discretizations) in mind, and some more elaborate versions are also implemented, namely arclength continuation in the initial states to pass around folds in α. See [dWU19] or [Uec21, Chapter 11] for algorithmic details. We write the PDE case (1.10) in condensed form for $u = u(x,t) = (v(x,t), \lambda(x,t)) \in \mathbb{R}^{2N}$ as

$$\partial_t u = -G(u) = g(u) + \mathcal{D}\Delta u, \text{ in } \Omega, \quad \text{with } \mathcal{D} = \begin{pmatrix} D & 0 \\ 0 & -D \end{pmatrix}, \quad v|_{t=0} = v_0 \tag{1.17}$$

together with the pertinent BCs for v and λ (here always Neumann BCs). In summary, to obtain solutions, we proceed in two steps:

1. First, we (numerically) compute CSSs (and their values) for (1.17). This is a more or less standard (though possibly elaborate) problem for an elliptic system, and can conveniently and efficiently be treated as a continuation and bifurcation problem by the package `pde2path` [UWR14, Uec21], which uses the finite element method (FEM) for the spatial discretization. The (branches of) CSSs can again be characterized as either flat (FCSS, i.e., spatially homogeneous), or patterned (PCSS, i.e., x–dependent). Moreover, also the saddle point property can be naturally generalized to the PDE case (1.10): After spatial discretization with n_p points we have an $n = 2Nn_p$–dimensional ODE (resp. algebraic system for CSSs), and we call a CSS $\hat{u}$ a saddle–point CSS if $\dim W_s(\hat{u}) = n$, and call $d(\hat{u}) = n - \dim W_s(\hat{u})$ the defect of $\hat{u}$. For small n_p (coarse meshes), $d(\hat{u})$ may depend on n_p, but for $n_p \to \infty$ this becomes mesh–independent, cf. [GU17].
2. In a second step, we again aim to compute canonical paths from some initial state v_0 to one or several SPP–CSSs $\hat{u}$ computed in the first step.

Remark 1.1. Numerically, the differences between (1.3), (1.6) and (1.10) are *quantitative* rather than *qualitative*. In particular, we also use `pde2path` for the bifurcation analysis of CSSs of (1.3) and (1.6), essentially by considering the 2P problem (1.6) as a "PDE-discretization" with

[4] By symmetry (spatial homogeneity), if $(\hat{v}_1, \hat{v}_2, \hat{\lambda}_1, \hat{\lambda}_2)$ is a PCSS, then so is $(\hat{v}_2, \hat{v}_1, \hat{\lambda}_2, \hat{\lambda}_1)$, and we generally do not distinguish these two

$n_p = 2$ discretization points. This then includes the 1P problem if we restrict to FCSSs (and flat canonical paths), which, moreover, can be used to check the *optimal diffusion–induced instability* (ODI) conditions (1.20) below, which give criteria if and where (primary) PCSSs (may) bifurcate. Considering the genuine PDE–setting (1.10), may require a large n_p (e.g., if $\Omega \subset \mathbb{R}^2$), and the numerics, in particular for canonical paths, become somewhat expensive. Nevertheless, our method works robustly and reasonably fast (on the order of minutes for the computation of canonical paths) up to a few thousand spatial degrees of freedom $n = Nn_p$. ⌋

1.2 Optimal Diffusion–induced Instability (ODI)

An important question for (1.6) and (1.10) is whether PCSSs exist. A seminal analysis has been put forward in [BX08], considering instabilities of FCSSs. For the case of scalar states, this yields conditions on the Jacobian

$$J^0 = \begin{pmatrix} H_{\lambda v} & H_{\lambda\lambda} \\ -H_{vv} & \rho - H_{v\lambda} \end{pmatrix} \tag{1.18}$$

of the "reaction part" $\partial_t u = (H_\lambda, \rho\lambda - \partial_v H)$ of (1.10) with $D = 0$ at some FCSS, where we dropped the $\tilde{}$ in the maximized Hamiltonian $\tilde{H}(v, \lambda) = H(v, \lambda, q(v, \lambda))$. These conditions describe the loss of the SPP at some parameter values and hence the possible bifurcation of (branches of) PCSSs, for suitable choice of $D > 0$, or equivalently, the domain size. They are somewhat similar to the conditions for the Turing instability [Tur52, Mur89] in a two–component reaction–diffusion system, but due to the OC background the instability is aptly named *optimal diffusion–induced instability* (ODI). In detail, we have two scalar functions,

$$h_1(\hat{u}) = 2H_{v\lambda}(\hat{u}) - \rho \quad \text{and} \quad h_2(\hat{u}) = \rho^2/4 - H_{\lambda\lambda}(\hat{u})H_{vv}(\hat{u}), \tag{1.19}$$

depending on the parameters, e.g., ρ, and the 1P CSS values $\hat{u}$ (which themselves depend on the parameters). Necessary conditions for a defect $d(\hat{u}) > 0$ of the FCSS $\hat{u}$ then are

$$h_1(\hat{u}) > 0 \text{ and } h_2(\hat{u}) > 0, \tag{1.20}$$

and thus we may for instance expect the bifurcation of a PCSS branch at a point on a FCSS branch where, e.g., $h_1 > 0$ and h_2 changes sign. These conditions only concern the FCSSs $\hat{u}$ itself, and hence can be checked analytically in some cases, but also numerically during the continuation of FCSSs in a 1P setting (or 2P setting, as explained in Remark 1.1), see the examples below.

In [BX08], the theory is then applied to three example problems, namely a shallow lake OC problem, and two optimal resource management problems. This means that the ODI conditions (1.20) are discussed for the respective problems, together with their economic interpretations. See also [BX10] for optimal harvesting in a 2–state vegetation–water system, which yields ODIs. However, the actual bifurcations of branches of PCSS, their possible defects, their canonical paths and ultimately their optimality are not discussed in [BX08, BX10]. As indicated above, this is in general a rather nontrivial numerical problem, but the computation of canonical paths is necessary to decide on optimality (or not) of a saddle–point CSS $\hat{u}$, and, in particular in case of optimality, to have the actual time-dependent control to govern the system from an initial state v_0 to $\hat{u}$.

1.3 The models, and preview of results

In [Uec16, GU17], the analysis from [BX08] (and [BX10]) is extended by a numerical bifurcation analysis of FCSSs and PCSSs for the shallow lake problem and the vegetation problem, in 1D and 2D, including the computation of canonical paths to FCSSs and PCSSs with the SPP, all based on `pde2path`. However, patterned *optimal* steady states (POSSs, in short) could not be found in the shallow lake model. For the vegetation–water system in [Uec16] we find large families of POSSs, but this is to some extent to be expected as already the uncontrolled reaction–diffusion system features Turing instabilities leading to pattern formation. In [GUU19], we use `pde2path` in a similar setup to study CSSs and canonical paths in OC of fisheries with boundary catch, which are hence a priori spatially inhomogeneous. Finally, in [UUHB21] genuine ODI pattern formation with POSSs is found in a scalar state PDE model FEED, modeling feeding, or, more generally, optimal stock–enhancement of a renewable resource, see below.

Here we complement these results by computing POSSs in two further scalar OC problems, namely one of the optimal resource management problems FISH from [BX08], and a pollution problem POLL based on [For75, TW96, Hed09]. Together with [UUHB21] this illustrates that pattern formation via ODI leading to POSSs can be seen as a generic phenomenon, occuring in open parameter sets in different classes of scalar PDE constrained OC problems, although some fine tuning of parameters is typically required. Moreover, while (1.20) is derived for the PDE case, we find it also convenient for the 2P versions of the models, and besides the PDE cases we discuss these in some detail, as they can be used to gain intuition and discuss domains of attraction. Another advantage of the 2P models is that [Tau15] applies for the rigorous derivation of the canonical system, while again we remark that the derivation of (1.10) is somewhat formal, but it yields results fully consistent with the case of discrete diffusion.

In §2 we review some results from [UUHB21] on the FEED model, and in §3 and §4 we discuss the FISH and POLL models and results, aiming at the spatial setting, but starting with the 1P canonical ODE systems, which, together with the ODI criterion (1.20) already give strong hints about the occurence of PCSSs, and their possible domains of attraction. In §5 we close with a brief summary and discussion. For comparison, here we collect J_c and the ODE right hand sides for the three models, i.e., for their 1P forms (1.1), namely

$$\text{FEED:}\quad J_c(v,a)=\log v-\frac{\gamma}{2}a^2,\quad \frac{\mathrm{d}}{\mathrm{d}t}v = av\,(1-v)-\delta v,\ \text{feeding rate } a \text{ as control;} \tag{1.21}$$

$$\text{FISH:}\quad J_c(v,E)=\alpha h-\frac{\beta}{2}h^2,\quad \frac{\mathrm{d}}{\mathrm{d}t}v = rv(1-v/K)-h,\quad h=Ev,\ \text{effort } E \text{ as control;} \tag{1.22}$$

$$\text{POLL:}\quad J_c(v,c)=\ln c-\frac{\gamma}{2}v^2,\quad \frac{\mathrm{d}}{\mathrm{d}t}v=\delta c-\beta v(\kappa-v)-m(1-v),\ \text{consumption } c \text{ as control.} \tag{1.23}$$

For FEED, we renamed the control q to a as it takes the form of an amplification of the natural growth rate of the stock v.[5] The first term in J_c is the utility of the stock, the second the costs of feeding; the term $av(1-v)$ models logistic growth with rate a and carrying capacity 1, while $-\delta v$ models the natural decay of v. For FISH, the control is the fishing effort E, such that $h=Ev$ is the harvest, and the (fish) stock has logistic growth with rate r and carrying capacity K. For POLL, the control is the consumption c, which drives the pollution stock v, but v is assimilated (or degraded) by the logistic function $-\beta v(K-v)$ with rate β and carrying capacity K, and additionally there are cleaning efforts $m(1-c)$ proportional to the part $1-c$ of the economy's output not used for consumption. The profit is similar to the one for FEED, but the roles of the

[5] Another motivation for naming the control a is that similar models appear in advertising, see [GCF+08, Ex.3.5], where a is the advertising effort, and v is the goodwill of customers (the willingness to buy a product).

control and the stock are reversed.

(a) FEED (b) FISH (c) POLL

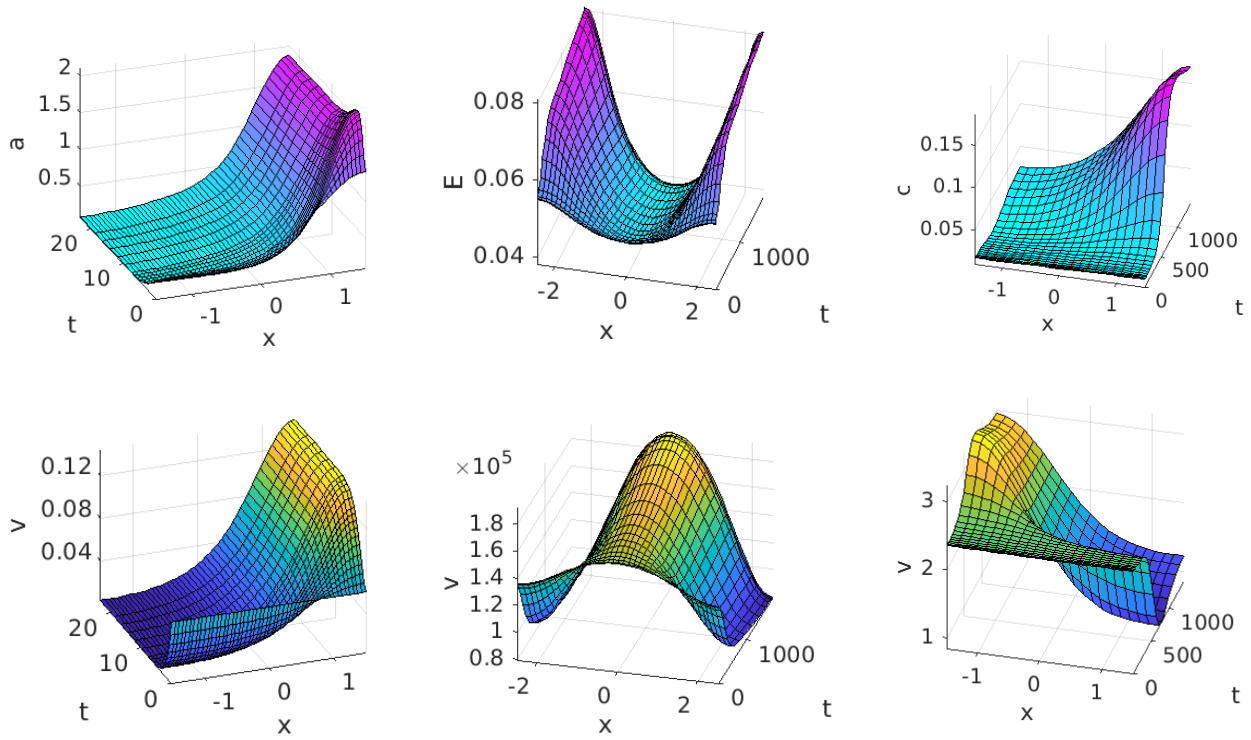

Figure 1.1: 1D sample canonical paths going to a PCSS (top: control, bottom: states). (a) FEED. In the PCSS (see (a) at $t = 20$), both, control a (feeding) and stock v, are large at the right boundary, and the canonical path goes from a FCSS to a PCSS. (b) FISH. The PCSS can be seen as a type of marine reserve, with little fishing effort E and high stock in the middle of the domain; however, the harvest $h = Ev$ is almost constant in the domain, see §3. (c) POLL. High pollution at the left, hence low consumption. In all three cases, the control of the system from the initial states maximizes the profit, and all three PCSSs can be considered as patterned *optimal* steady states (POSSs).

All three models share logistic growth (decay for POLL) of the stock, and J_c fulfills the typical assumptions on objective functions such as concavity in v and q, and for FEED (POLL) infinite marginal values at v=0 (at $c = 0$), i.e., $\partial_v J_c(0, a) = \infty$ ($\partial_c J_c(v, 0) = \infty$). Of course, for instance for FEED also $\lim_{v \searrow 0} J_c(v, a) = -\infty$, and the current value $J_c(v, a)$ (and hence also the total value $J(v, a) = \int_0^\infty \mathrm{e}^{-\rho t} J_c(v, a)\, \mathrm{d}t$) can (and typically will) be negative, but this is only a question of offset. What matters is the comparison of J for different controls a. In Fig. 1.1 we show a POSS and an associated canonical path for each of the three models, but refer to the further sections for discussion, parameter values, and domains and diffusion constants for the spatial models.[6] There we also give a few modeling and economic comments, but otherwise take the models as given and focus on the mathematical (numerical) methods and results.

[6]In FEED and POLL we shall have dimensionless parameters, chosen for convenience and clarity of results; for FISH we use the dimensional parameters from [BX08]. At this point we only remark that in all three models we have ρ near 0.03, which means that the unit of t should be thought as years. In particular, for FISH and POLL in Fig. 1.1 we then have a very long time horizon for the approach to the POSSs, which is essentially due to a small stable eigenvalue μ_1, cf. (1.15).

2 Optimal feeding

To set the stage for the fishing and pollution models in §3 and §4, we review some results from [UUHB21] on the FEED model. The dynamics and J_c are given in (1.21), i.e.,

$$J_c(v,a) = \log v - \frac{\gamma}{2}a^2, \quad \frac{\mathrm{d}}{\mathrm{d}t}v = f(v,a) := av\,(1-v) - \delta v, \tag{2.1}$$

The control a is the growth rate (feeding) of the stock v, which gives the utility[7] $\log v$ in J_c, but feeding costs money, modeled by $-\frac{\gamma}{2}a^2$ in J_c. Applying Pontryagin's Maximum Principle to the spatial problem yields the canonical system

$$\partial_t v = \frac{\lambda}{\gamma}v^2(1-v)^2 - \delta v + D\Delta v, \qquad v|_{t=0} = v_0, \tag{2.2a}$$

$$\partial_t \lambda = \lambda(\delta+\rho) - \frac{1}{\gamma}\lambda^2 v(1-2v)(1-v) - \frac{1}{v} - D\Delta\lambda, \tag{2.2b}$$

with $a = \lambda v(1-v)/\gamma$ (pointwise in x and t), and with Neumann BCs for v and λ. For the 1P problem we have $(v,\lambda) = (v,\lambda)(t)$, dropping the $D\Delta$ terms, and for the 2P problem we replace these by discrete diffusion.

Besides the existence of PCSSs for (2.2), a remarkable feature are their rather large domains of attraction, which we shall discuss (also for the FISH and POLL models) in the 2P setting. Recall from (1.13) that given a $2n$ dimensional canonical system with possibly several CSSs $\hat{u}$, the domain of attraction of a CSS $\hat{u} \in \mathbb{R}^{2n}$ is the set

$$\mathcal{A}(\hat{u}) := \{v_0 \in \mathbb{R}^n : \text{there exists, by choice of } \lambda_0 \in \mathbb{R}^n, \text{ a canonical path from } v_0 \text{ to } \hat{u}\}.$$

A CSS $\hat{u}$ is called *globally stable* if $\mathcal{A}(\hat{u}) = \mathbb{R}^n$ (or if $\mathcal{A}(\hat{u}) = \mathcal{B}$ if the dynamics is restricted to some subset $\mathcal{B} \subset \mathbb{R}^n$, e.g., $\mathcal{B} = \mathbb{R}^n_+$). More generally, a CSS $\hat{u}$ may be considered important if $\mathcal{A}(\hat{u})$ is "large" in a suitable sense. These definitions do not involve the optimality of a canonical path, and if several CSSs exist, then their domains of attraction may have non–empty intersections. Then, given an initial state $v_0 \in \mathcal{A}(\hat{u}^{(a)}) \cap \mathcal{A}(\hat{u}^{(b)})$, the first step is to compare the value $J(v_0;\hat{u}^{(a)})$ of the canonical path to $\hat{u}^{(a)}$ with the value $J(v_0;\hat{u}^{(b)})$ of the canonical path to $\hat{u}^{(b)}$.

In Fig. 2.1 we summarize results for (2.2), with base parameter set

$$(\rho, m, \beta, \gamma) = (0.015, 0.01, 0.01, 0.01) \tag{2.3}$$

and bifurcation parameter δ, with many more details and economic discussion given in [UUHB21]. (a) shows a phase portrait for the 1P version with $\delta = 0.3$, with the unique fixed point $\hat{u}$ marked by the red dot. This is a saddle point, and its stable (unstable) manifold is given by the green (red) lines. The dashed lines are the nullclines, and the blue lines are selected orbits. The phase portrait shows that $\hat{u}$ is globally stable: For any $v_0 > 0$, we find a unique λ_0 such that (v_0,λ_0) is on $W_s(\hat{u})$ (on the green line), and this uniquely determines the canonical path from v_0 to $\hat{u}$. In particular, $W_s(\hat{u})$ extends to large v_0 and is "well behaved" there (this will be different for the other models). It also extends to small v_0, but becomes rather steep with large λ; this agrees with economics, as small stocks have large "shadow prices" λ, and in particular $\lambda \to \infty$ on $W_s(\hat{u})$ as $v \to 0$, due to $-1/v$ in (2.2b), which is a consequence of the infinite marginal value in J_c at $v = 0$ from $\log v$.

[7] not necessarily as food; the utility may as well be, e.g., benefits for the eco–system, i.e. nature preservation

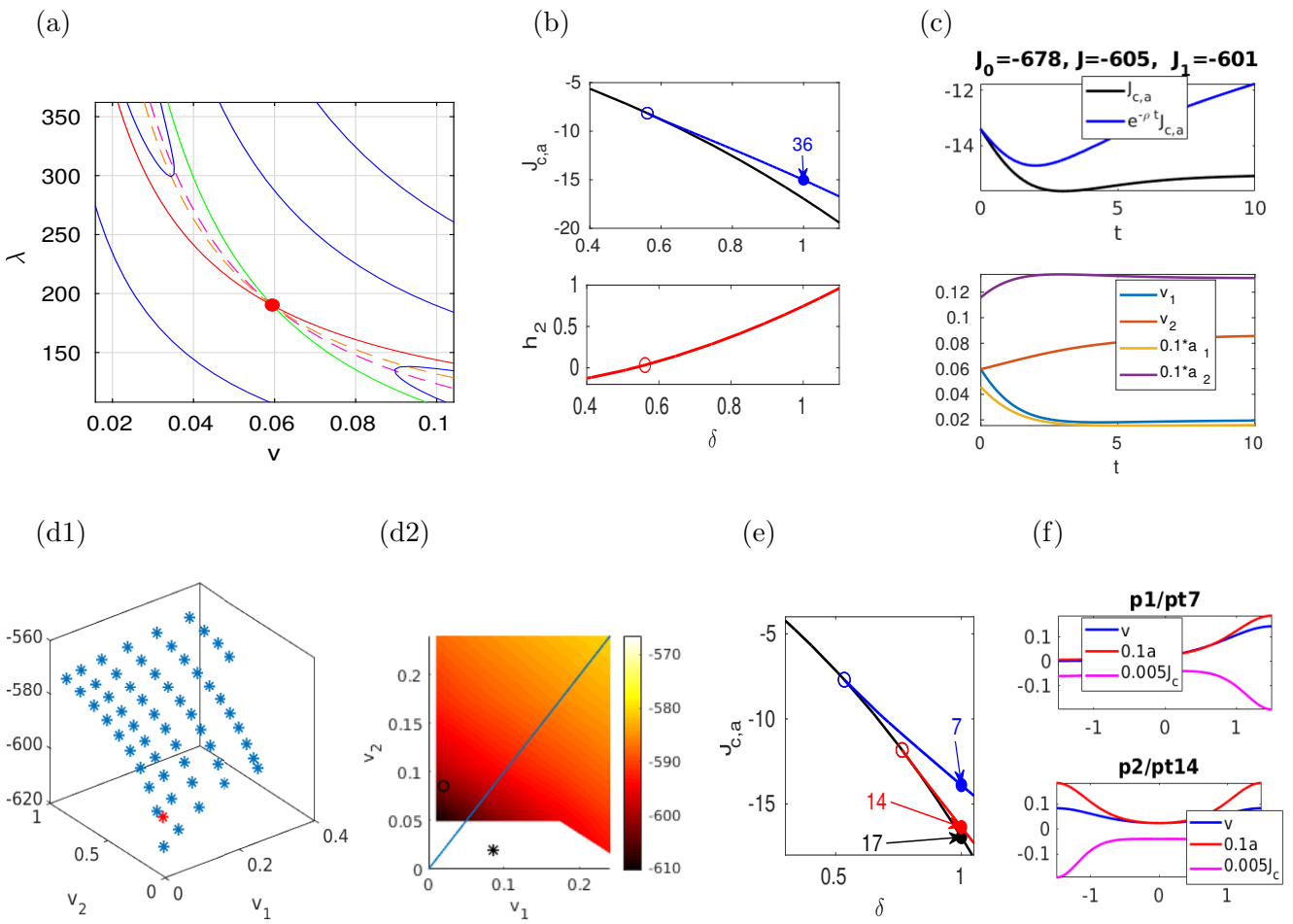

Figure 2.1: (a) One patch phase portrait for FEED, parameters (2.3), $\delta = 0.3$. (b) Top panel: 2P continuation in δ with $D = 0.25$, with the black branch correponding to the FCSS, and the blue branch a PCSS. Bottom: ODI indicator function h_2 along the black branch. (c) canonical path FCSS to p1/pt36. (d) values of p1/pt36. (e,f) 1D bifurcation diagram and sample solutions, $D = 0.25$.

In Fig. 2.1(b–d) we turn to the 2P model, using δ as a continuation and bifurcation parameter for steady states. The black line (which is independent of D) in the top panel in (b) shows $J_{c,a}$ for the FCSS, and the bottom panel (red line) the ODI indicator function h_2 from (1.20), which shows that (for suitable choice of D) we obtain an ODI around $\delta = 0.56$ (h_1 is always positive).[8] Choosing $D = 0.25$ we obtain the bifurcation of the blue PCSS branch at $\delta \approx 0.565$. This has the SPP, and at $\delta = 1$ we numerically obtain $\hat{u} = (v_1, v_2, \lambda_1, \lambda_2) \approx (0.02, 0.085, 82, 166)$. In (c) we then show a canonical path to $\hat{u}$, starting at $v_0 \approx (0.06, 0.06)$ (from the FCSS at $\delta = 0$). The top panel shows $J_{c,a}$ and $\mathrm{e}^{-\rho t} J_{c,a}$ along the canonical path, and the numbers

$$J_0 = -678, J = -605, J_1 = -601 \tag{2.4}$$

give the values of the FCSS, of the canonical path, and of the target PCSS, respectively, using (1.16) for the canonical path. The numbers (2.4) show that we can substantially increase the profit by controling the system from the FCSS to the PCSS. The bottom panel in (c) shows v and a along the canonical path; to control the system from the FCSS to the PCSS (with $v_2 > v_1$), we start with $a_2 > a_1$, and the convergence to the PCSS is monotone and rather fast.

[8]Here and in the following, open circles in bifurcation diagrams (BDs) such as Fig. 2.1(b,top) or (e) indicate bifurcation points. Numbers on branches indicate specific points on the branch, typically subsequently plotted, like `pt7` on the blue branch `p1`, and `pt14` on the red branch `p2`, in (f).

In Fig. 2.1(d) we characterize the domain of attraction of the PCSS $\hat{u}^{\rm PCSS}$ (at $\delta = 1$), by sampling the initial states plane $v_0 = (v_{0,1}, v_{0,2})$ and aiming (see Remark 2.1 for the algorithm) to compute canonical paths to $\hat{u}^{\rm PCSS}$, indicated by the red $*$ in (d1) and the open circle in (d2). By symmetry, cf. Footnote 4, if $\hat{u}$ is a PCSS, then so is $M\hat{u} = (v_2, v_1, \lambda_2, \lambda_1)$. In (d2), obtained from a Delaunay triangulation of (d1), we also mark $M\hat{u}^{\rm PCSS}$, and indicate the diagonal by the blue line. The main conclusions from (d) are as follows:

- $\mathcal{A}(\hat{u}^{\rm PCSS})$ extends to large $v_{0,1}$ and $v_{0,2}$, and $J(v_0)$ is monotonously increasing in $v_{0,1}$ and $v_{0,2}$.
- For non–small $v_{0,2}$, $\mathcal{A}(\hat{u}^{\rm PCSS})$ contains $v_{0,1}$ values beyond the diagonal. However, the mirrored PCSS $M\hat{v}$ is not in $\mathcal{A}(\hat{u})$, i.e., a canonical path from $M\hat{v}^m$ (see the $*$ in (d2)) to $\hat{u}^{\rm PCSS}$ does not exist. Nevertheless, $\mathcal{A}(\hat{u}^{\rm PCSS})$ and $\mathcal{A}(M\hat{u}^{\rm PCSS})$ have a large intersection. As $J(v_0; M\hat{u}^{\rm PCSS})$ can be obtained from mirroring $J(v_0; \hat{u}^{\rm PCSS})$ across the diagonal, $\mathcal{A}(\hat{u}^{\rm PCSS}) \cap \{v_1 = v_2\}$ forms an obvious Skiba manifold [Ski78] for the 2P problem: Above (below) the diagonal it is optimal to go to $\hat{u}^{\rm PCSS}$ (to $M\hat{u}^{\rm PCSS}$).

Remark 2.1. In Fig. 2.1(d) we use a fixed truncation time $t_0 = 20$ for (1.14), and also a fixed stepsize for the continuation algorithm in α for the continuation of canonical paths in the initial states. If this yields a canonical path at $\alpha = 1$, then we store v_0 and $J(v_0)$ in an array, and this gives the blue dots in (d1). As a result, $\mathcal{A}(\hat{u}^{\rm PCSS})$ contains *at least* (the v_0 values of) the dots in (d1). In fact, by finer sampling of the v_0 plane and fine tuning the canonical path computation we can slightly increase the numerical $\mathcal{A}(\hat{u}^{\rm PCSS})$, but altogether the characterization in (d) seems somewhat sharp. ⌋

In summary, (d), together with similar computations at other parameter values, illustrates that for the FEED 2P problem we have a large $\mathcal{A}(\hat{u}^{\rm PCSS})$. This will be quite different for the FISH and POLL problems studied below. Intuitively, we attribute the large $\mathcal{A}(\hat{u}^{\rm PCSS})$ for FEED to the "well–behaved" (1D) stable manifold in the 1P problem; the analogous stable manifolds in the FISH and POLL problems will turn out to be much less well-behaved.

Figure 2.1(e,f) shows the bifurcation diagram for the 1D PDE case with $\Omega = (-1.5, 1.5)$ and $D = 0.25$. The blue branch contains PCSSs with the SPP and wave number $k = 0.5$ (see top panel in (f) for a sample solution), and it bifurcates close to $\delta = 0.56$ as predicted by the ODI criterion $h_2 > 0$, i.e., the sign change of h_2. The red branch contains PCSSs with wave number $k = 1$ (see bottom panel in (f)), which have defect $d = 1$. The PCSSs on the blue branch again have quite large domains of attraction, although a precise characterization as in (d) for the 2P case is no longer feasible for the now infinite dimensional (or, after spatial discretization, high dimensional) phase space. In any case, the FCSS is in the domain of attraction of the blue PCSS for all $\delta > \delta_0$, and in Fig. 1.1(a) we show the canonical path from FCSS/pt17 to p1/pt7. For the values we have

$$J_0 \approx -678 \text{ (FCSS)}, \; J \approx -556 \text{ (canonical path)}, \text{ and } J_1 \approx -555 \text{ (target PCSS)}, \tag{2.5}$$

showing that going to the PCSS can significantly increase the profit compared to, e.g., staying in the FCSS.

Remark 2.2. a) While we have *not* actually proved that the CSSs from Fig. 2.1 with the SPP are (locally) optimal (as we assumed sufficient smoothness of optimal solutions and the pertinent inter–temporal transversality conditions), we believe that this holds beyond reasonable doubt, and hence they are patterned *optimal* steady states (POSSs).

b) See [UUHB21] for results for (2.2) in 2D, and more elaborate bifurcation diagrams including secondary bifurcations. This yields further PCSS branches and in particular multiple PCSSs with the SPP, and each of these saddle–point PCSSs has a non–small domain of attraction. ⌋

3 Optimal fishing and marine reserves

In the model (1.22), following [BX08, §5.2.1.1], v is the biomass of fish, for which we assume logistic growth with rate r and carrying capacity K. The catch (or harvest) is $h = h(E, v) = Ev$ with harvesting effort E as control, and the local current value is $J_c(h) = \alpha h - \frac{\beta}{2}h^2$. The spatially continuous model is, to recall, with $f(v, E) = rv(1 - v/K) - Ev$,

$$J_c(h) = \alpha h - \frac{\beta}{2}h^2, \quad h = h(E, v) = Ev \text{ with effort } E \text{ as control}, \tag{3.1a}$$

$$\partial_t v = f(v, E) + D\Delta v, \quad x \in \Omega, t \geq 0, \quad \partial_n v|_{\partial\Omega} = 0, \quad v|_{t=0} = v_0, \tag{3.1b}$$

Remark 3.1. The model (3.1) with $J_c = J_c(h)$ which depends only on h, but not separately on v and E, appears somewhat oversimplified. In reality, we may for instance expect that J_c also depends on E, e.g., $J_c = \alpha h - \beta h^2/2 - \gamma E$ with $\gamma > 0$, as the effort itself also costs money. However, for $\gamma = 0$ the algebra is much simpler, and, moreover, the results stay qualitatively the same for $\gamma > 0$ (up to $\gamma = 10^8$ for the other parameters chosen below), and hence we stick to the original model. ⌋

We use the discount rate ρ as the bifurcation parameter, and otherwise essentially the parameter specifications from [BX08], namely[9]

$$(r, K, \alpha, \beta) = (0.08, 400\,000, 75\,000, 10), \tag{3.2}$$

were we changed α from 80 000 ([BX08]) to α=75 000 for graphical reasons, i.e., to better distinguish branches. Due to the dimensional parameters, and to gain intuition, in Fig. 3.1(a) we give simple plots of $J_c(h)$ and $f(v, E)$, in pertinent regimes. Obviously, J_c is maximal at $h_* = \alpha/\beta = 7500$, and $f(v, 0)$ is positive for $v \in (0, K)$. For instance for $v_* = 1.5 * 10^5$ we may then aim to choose $E = E_* = 0.05$ to have $h = Ev = h_*$, and this corresponds to a fixed point of $\frac{\mathrm{d}}{\mathrm{d}t}v = f(v, E)$. Similarly, for $v < v^*$ we may aim at $E > E_*$ to still have the harvest h_* which maximizes J_c. Then, however, we may have $\frac{\mathrm{d}}{\mathrm{d}t}v = f(v, E) < 0$, and it remains to be seen how to exactly choose E optimally.[10]

We apply Pontryagin's Maximum Principle and obtain $E = \dfrac{\alpha - \lambda}{\beta v}$, and the canonical system

$$\partial_t v = f(v, E) + D\Delta v, \quad v|_{t=0} = v_0, \tag{3.3a}$$

$$\partial_t \lambda = (\rho - \partial_v f(v, E))\lambda - D\Delta\lambda. \tag{3.3b}$$

The associated 1P model is (3.3) with $(v, \lambda) = (v, \lambda)(t) \in \mathbb{R}^2$ and the Δv and $\Delta\lambda$ terms dropped, and in the 2P model we have $(v, \lambda)(t) = (v_{1,2}, \lambda_{1,2})(t) \in \mathbb{R}^4$ with Δv and $\Delta\lambda$ denoting discrete diffusion. The pertinent FCSS is

$$\hat{u} = (\hat{v}, \hat{\lambda}) = \left(\frac{K(r - \rho)}{2\rho}, \frac{r(2\alpha - K) + \rho K}{\beta r(r + \rho)}\right), \tag{3.4}$$

[9] The values for (r, K) are from [Cla90, p49], corresponding to the antarctic fin-whale, with units $[r] = 1/y$, $[K] = w = \#$of whales, and consequently $([\alpha], [\beta], [\rho]) = (\$/w, \$y/w, 1/y)$.

[10] For instance, we might simply choose $E = h_*/v$ leading to the constant harvest h_*. This leads to extinction of v in finite time t_*, i.e., $\lim_{t\to t_*} v(t) = 0$, and, importantly, turns out not to be optimal, see Remark 3.2.

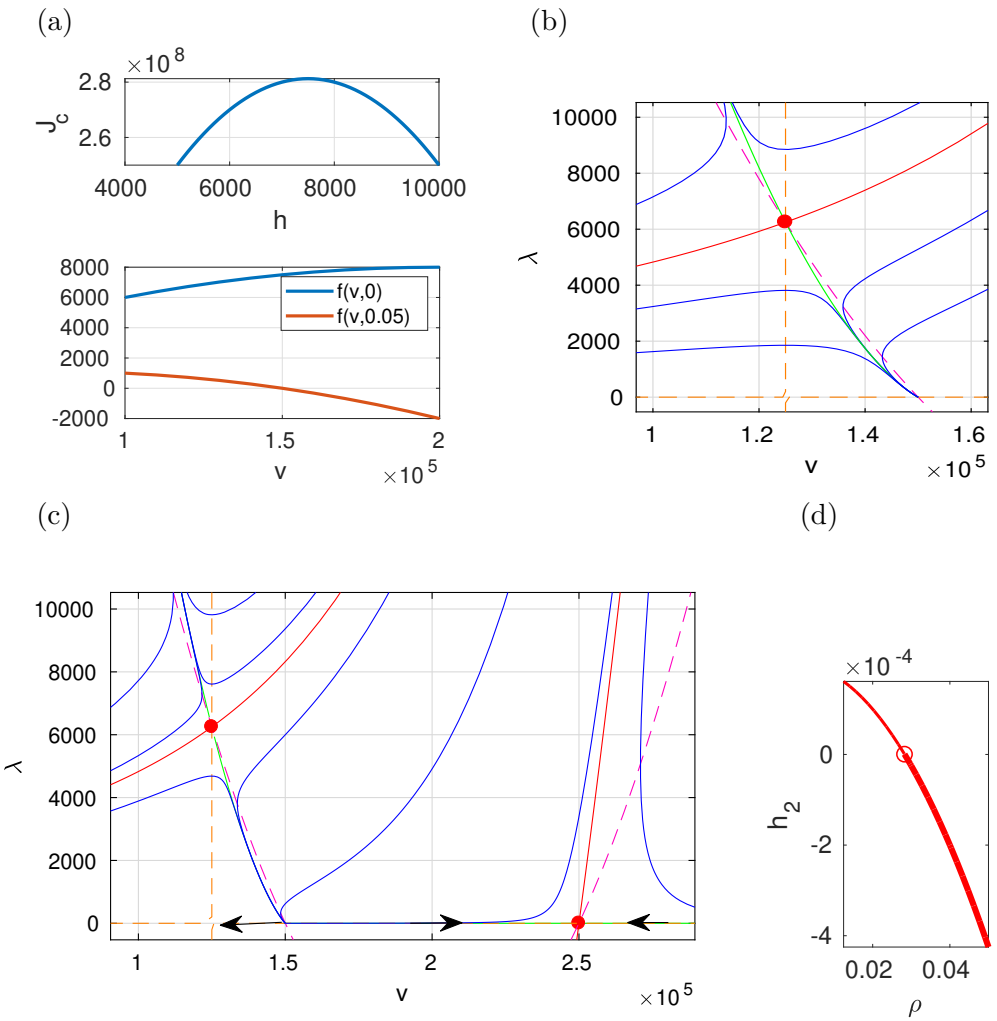

Figure 3.1: FISH. (a) Plots of $J_c(h)$ and of $f(v, E)$ for illustration. (b) Phase portrait for the 1P problem near the nontrivial CSS, $\rho = 0.03$. (c) The larger scale phase portrait; two saddle points (red dots), and an unstable node at $(v, \lambda) = (150000, 0)$; the black arrows indicate the flow on the invariant $\lambda = 0$ axis. (d) The ODI indicator function h_2 for continuation of the CSS from (a) in ρ.

and the ODI condition (1.20) for (3.3) is

$$h_2 = \frac{\rho^2}{4} - f''(\hat{v})\lambda^*/Q''(\hat{v}) = \rho^2/4 - 2r\hat{\lambda}/(\beta K) > 0, \tag{3.5}$$

as here $f'' = -2r/K$ and $Q'' = -\beta$ are independent of v and λ. Using (3.4), this can in principle be evaluated analytically, but instead, as in the FEED model, we just compute h_2 (and h_1, which is always positive) while continuing the FCSS (3.4) in parameters.

Figure 3.1(b) shows the phase portrait for the 1P problem, locally near the CSS (3.4), and (c) gives a more global picture. For $\rho > 0.01$, the 1P CSS (3.4) (red dot) is a saddle, with stable (unstable) manifolds $W_s(\hat{u})$ ($W_u(\hat{u})$) in green (red). Importantly, the southeast part of $W_s(\hat{u})$ is a heteroclinic orbit connecting for $t \to -\infty$ to a second (trivial) FP $\hat{u}^* = (\hat{v}^*, 0)$ with

$$\hat{v}^* = K/2 - \sqrt{K^2/4 - K\alpha/(r\beta)}, \tag{3.6}$$

($\hat{v}^* = 150000$ in Fig. 3.1(a,d)), with defect $d = 1$, and there is a third FP $\hat{u}^\circ = (\hat{v}^\circ, 0)$ with

$$\hat{v}^\circ = K/2 + \sqrt{K^2/4 - K\alpha/(r\beta)} \tag{3.7}$$

($\hat{v}^\circ = 250000$ in Fig. 3.1(b)), which is again a saddle. An immediate consequence of this phase portrait is that for the 1P problem with initial states $v_0 > \hat{v}^*$ a canonical path to $\hat{u}$ does not exist. Instead, the only CSS that can be reached is $\hat{u}^\circ$, and the canonical path has $\lambda \equiv 0$ and hence $E = \alpha/(\beta v)$, i.e., the constant harvest $h = \alpha/\beta$. All this agrees with the intuition gained from (a), and the 1P domain of attraction of $\hat{u}$ being bounded above by $\hat{v}^*$ means that for the spatial problems (2P or PDE) we should not expect large domains of attraction of (saddle point) PCSSs. See below for further discussion. In (d) we plot h_2 from (3.5), showing that we have an ODI at $\rho_0 \approx 0.028$.

In Fig. 3.2 we consider the 2P problem with $D = 2/300$, starting with the black FCSS branch as a function of ρ. In (rough, since we did not optimize for D) agreement with Fig. 3.1(d), at $\rho \approx 0.027$ a PCSS branch (`b1`, blue) bifurcates from the FCSS $\hat{u}^{\text{FCSS}} = (\hat{u}, \hat{u})$ towards larger ρ, with a fold at $\rho = \rho_f \approx 0.048$, where it gains the SPP.[11] At `b1/pt15` ($\rho = 0.04$),

$$\hat{u}^{\text{PCSS}} \approx (85900, 191000, 14020, 2170), \text{ and } (E_1, E_2) \approx (0.07, 0.038), \tag{3.8}$$

which means that patch 2 can be interpreted as a *marine reserve* (which turns out to be optimal, see below): In patch 2 we have a smaller fishing effort E_2 and a larger fish stock v_2. However, the harvest $h = Ev = 10^3(6.1, 7.28)$ is actually larger in patch 2 than in patch 1, and intuitively, the reason for $J(\hat{u}^{\text{PCSS}}) > J(\hat{u}^{\text{FCSS}})$ is that for $\hat{u}^{\text{PCSS}}$ the harvest in patch 2 is closer to the optimal $h_* = 7500$. Given the larger v_2, this is achieved by a small effort E_2, and at the same time v being maximal in patch 2 yields diffusion to patch 1 which keeps the large v_2 in steady state. The converse arguments apply to patch 1, where (after the fold) we also have h_1 closer to h_* than in the FCSS.

The subcritical bifurcation of `b1` yields a range $\rho \in (\rho_1, \rho_f)$ where both, the FCSS and the PCSS have the SPP, and it is interesting to compare their domains of attraction and values. In (b,c) we show two canonical paths from initial states $v_0 = 10^5(0.5, 1.5)$, which are chosen rather carefuly (by trial and error) to be in $\mathcal{A}(\hat{u}^{\text{FCSS}}) \cap \mathcal{A}(\hat{u}^{\text{PCSS}})$. In (b) we target the FCSS with $J_1 := J(\hat{u}^{\text{FCSS}}) \approx 6.75 * 10^9$, and obtain $J = 6.3921 * 10^9$ for the canonical path. In (c), we target $\hat{u}^{\text{PCSS}}$ with $J_1 = 6.91 * 10^9$, and obtain a slightly larger $\tilde{J} = 6.3924 * 10^9$ for the canonical path. However, $\tilde{J} = J$, up to 4 digits, which shows that for this v_0 the difference between going to the PCSS and the FCSS is rather marginal, although the FCSS has a somewhat smaller CSS value. Naturally, for going to the FCSS the harvesting efforts become equal for $t \to \infty$; for going to the PCSS, we have $E_1(t) > E_2(t)$ throughout, and E_1, E_2 are monotonously increasing/decreasing. If, e.g., $v_0 = 10^5(1.5, 0.5)$, then we would of course target the mirrored PCSS $M\hat{u}^{\text{PCSS}} \approx (191000, 85900, 2170, 14020)$.

However, altogether the domains of attraction of both, the FCSS and the PCSS, are not large, and, moreover, have a small intersection, see (d). This can be related to the 1P phase portrait. As discussed above, the 1P domain of attraction of the FCSS is bounded above by $\hat{v}^*$, and this is essentially inherited by the 2P domain of attraction of $\hat{u}^{\text{FCSS}}$: Canonical paths to $\hat{u}^{\text{FCSS}}$ only exist for $\max(v_{0,1}, v_{0,2}) \leq \hat{v}^* + \delta$, where δ depends von D, but is small compared to $\hat{v} \approx 10^5$, i.e., $\delta \leq 10^3$ in our experiments. Otherwise, $J(v_0)$ is as expected, i.e., monotonously increasing in v_1 and v_2.

For $v_{0,1}$ near 10^5, canonical paths to $\hat{u}^{\text{PCSS}}$ also exist for larger $v_{0,2}$ ($v_{0,2} = 3 * 10^5$, say) but not

[11] We continue these branches as long as $\lambda_{1,2} \geq 0$, which for both, the FCSS and the PCSS, gets violated near $\rho = 0.02$.

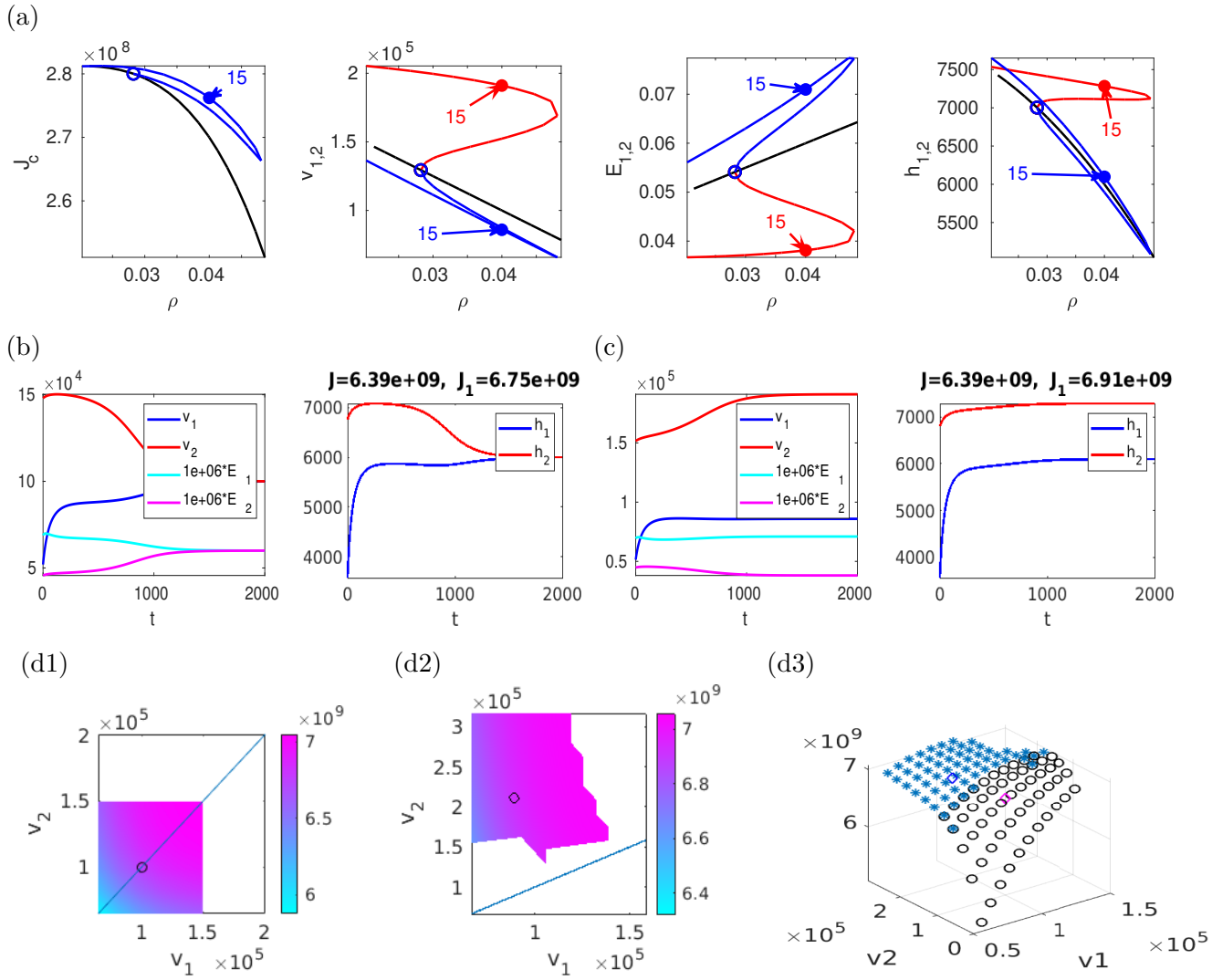

Figure 3.2: FISH 2P. (a) bifurcation diagrams. FCSS branch (black), and PCSS branch (blue, respectively blue (patch 1) and red (patch2)). (b,c) canonical paths to $\hat{u}^{\mathrm{FCSS}}$ and $\hat{u}^{\mathrm{PCSS}}$ at $\rho = 0.04$, both starting from $\hat{v}_0 = 10^5(0.5, 1.5)$, and both giving almost equal values $J \approx 6.39 * 10^9$, while $J(\hat{u}^{\mathrm{FCSS}}) < J(\hat{u}^{\mathrm{PCSS}})$. (d) value diagrams for the FCSS (d1) and the PCSS (d2) at $\rho = 0.04$, and both together in (d3).

for "small" $v_{0,2}$, see (d2). On the (small) intersection of these numerical $\mathcal{A}(\hat{u}^{\mathrm{PCSS}})$ and $\mathcal{A}(\hat{u}^{\mathrm{FCSS}})$, the canonical paths to $\hat{u}^{\mathrm{PCSS}}$ yield a slightly larger J than for the canonical paths to $\hat{u}^{\mathrm{FCSS}}$. However, due to a small stable eigenvalue μ_2, cf. (1.15), the approach to the target PCSS is rather slow with a time horizon of at least 1000 years. For the canonical paths at $\rho = 0.04$ (annual discount rate) we obtain a significant contribution to J only for $t < t_1$ with $t_1 = 10/\rho = 250$ (years), as $\mathrm{e}^{-\rho t} < \mathrm{e}^{-10} \approx 4.5 * 10^{-5}$ for $t > t_1$, such that the long–time control to reach the PCSS hardly matters. This means that our method may not be practically useful for the model, but nevertheless we obtain a proof–of–principle for *optimal* marine reserves.

Remark 3.2. As a sanity check, Fig. 3.3 shows what happens for the greedy overfishing choice $E(t) = h_*/v(t)$, i.e., $h(t) \equiv h_*$, by simple time integration of the 1P model (1.22). For any $v(0) < \hat{v}^* = 1.5 * 10^5$ we have $v(t) \searrow 0$ in finite time t_* (panel (a)), with $\lim_{t \to t_*} E(t) = \infty$, which in any case is unrealistic, cf. Remark 3.1. However, even though the effort E is for free (on h appears in J_c), the choice $E(t) = h_*/v(t)$ is not optimal. As $J_c = J_* = \alpha h_* - \beta h_*^2/2$ is constant, the value of the choice is $J = \int_0^{t_*} J_* \mathrm{e}^{-\rho t} \, \mathrm{d}t = J_*(1 - \mathrm{e}^{\rho t_*})$, which is below the values of the canonical

paths to $\hat{u}^{\mathrm{FCSS}}$, see panel (b). Similar results can be obtained for greedy ad hoc choices in the 2P models. ⌋

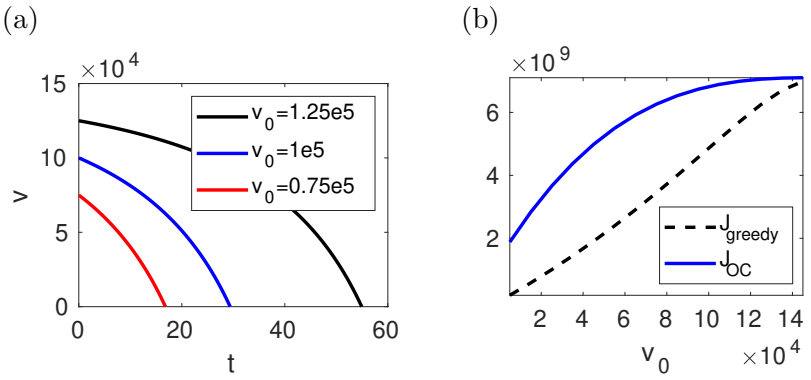

Figure 3.3: Dynamics (a) and values (b) for the greedy overfishing choice $E(t) = h_*/v(t)$ for (1.22), leading to extinction of v in finite time, and yielding suboptimal values $J(v_0)$, see Remark 3.2.

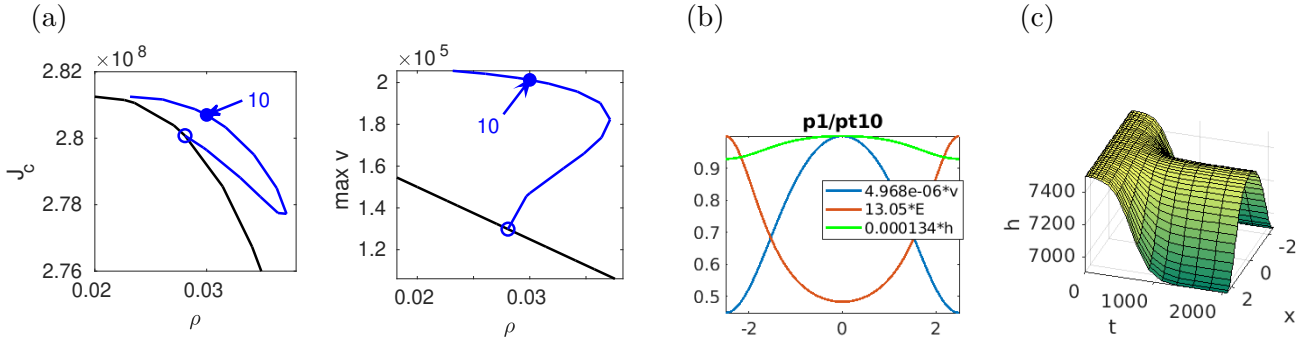

Figure 3.4: FISH 1D, $\Omega = (-2.5, 2.5)$, $D = 0.01$, other parameters as before. (a) bifurcation diagrams. (b) PCSS sample solution. (c) h on the canonical path to the PCSS (see Fig. 1.1(b) for E and v), starting near (but not in) the $\hat{v}$ from the FCSS.

In Fig. 3.4(a) we give bifurcation diagrams for the 1D PDE case, choosing $\Omega = (-2.5, 2.5)$ and $D = 0.01$. The black branch represents $\hat{u}^{\mathrm{FCSS}}$ and at $\rho \approx 0.0275$ the blue PCSS branch bifurcates, with a sample solution at $\rho = 0.03$ in (b). Again the PCSS has the SPP after the fold; from just v and E, it has a nice interpretation of an at least locally optimal marine reserve, with low fishing and high stock now in the middle of the domain. However, again the harvest h is actually larger in the middle (the reserve) than at the boundaries. The domains of attraction of these PCSSs are not very large, and we refer to Fig. 1.1(b) for an example canonical path to `b1/pt10`, with initial state close to $v \equiv 1.5 * 10^5$, which yields $J = 7.04 * 10^9$, while $J(\hat{u}^{\mathrm{PCSS}}) = 6.96 * 10^9$. Figure 3.4(d) shows the harvest along the canonical path.

In Fig. 3.5 we give results for (3.3) on a square domain. This 2D case naturally gives a richer bifurcation diagram of PCSS. The black branch is again the FCSS, and at the first branch point at $\rho \approx 0.027$ we have a two–dimensional kernel, spanned by, e.g., vertical and horizontal stripes. By symmetry ([GS02, Hoy06], and [Uec21, §2.5]), we then have two (isotropy classes of) bifurcating branches, namely stripes (b) (same as in 1D in Fig. 3.4, on half the domain) and spots (c), where the latter in lowest order correspond to an equal amplitude superposition of vertical and horizontal stripes. The stripes extend to $\rho \approx 0.037$ and have $d = 0$ between the fold and the next secondary branch point at $\rho \approx 0.032$, while the spots extend to larger ρ but are unphysical there as they

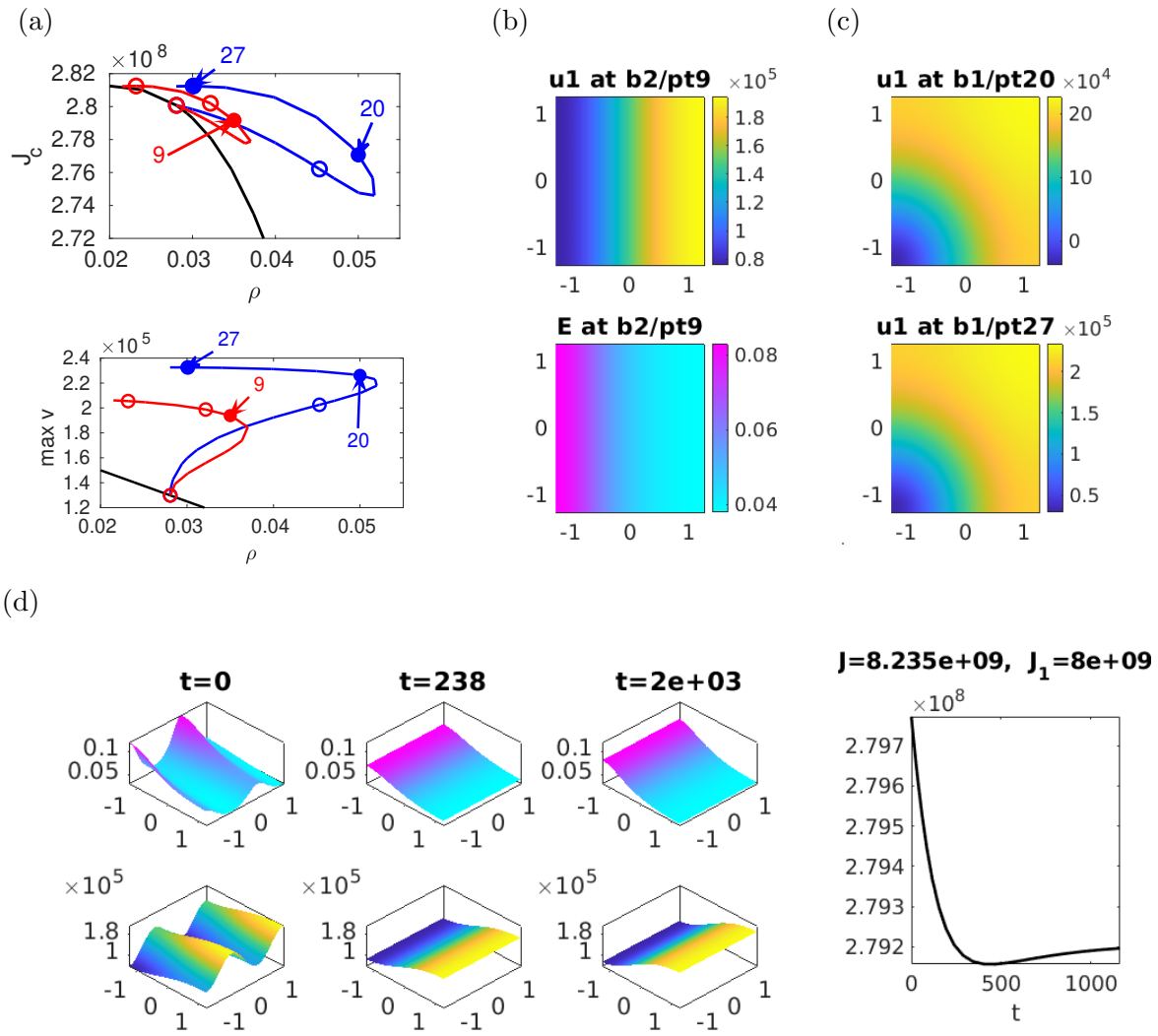

Figure 3.5: FISH on $\Omega = (-l_x, l_x)^2$, $l_x = 1.25$, with $D = 0.01$. (a) bifurcation diagram, J_c and $\max v$ over ρ, FCCS branch (black), and two primary PCSS branches, spots (`b1`, blue), and stripes (`b2`, red). (b,c) A sample stripe, with E, and a sample spot, unphysical at pt20 (`u1` means v). (d) canonical path to b2/9, top row E, bottom row v, with t as indicated. Right: J_{ca} along the canonical path, with value $J = 8.235 * 10^9$, and value $J_1 = 8.0002 * 10^9$ of the target.

feature negative v, see the first plot in (c). Altogether, all spots are either unphysical ($v < 0$ in part of the domain) or unstable ($d \geq 1$), or both. In (d) we thus content ourselves with illustration of one canonical path to the stripe at $\rho = 0.035$, from a v_0 which has some y modulation. On this canonical path, it may again appear counter–intuitive that from the start the larger effort E (top row) is at low v (bottom row), but this again can be explained by the system aiming to have the harvest close to the optimum $h_* = 7500$, everywhere in x and t on the canonical path.

4 Optimal pollution

Production and consumption of goods may lead to pollution, and choosing an optimal trade–off between utility of consumption and disutility (costs) of pollution is a classical and much studied problem in OC, see, e.g., [For75, TW96, Hed09], and the references therein. Here we extend the modification (1.23) of the model from [TW96] to a spatial setting. The consumption

$c : \Omega \times [0, \infty) \to \mathbb{R}_+$ is the control, and the pollution stock $v = v(x, t) \geq 0$ evolves according to

$$\partial_t v = \delta c - a(v) - m(1 - c) + D\Delta v, \tag{4.1}$$

where $a : \mathbb{R}_+ \to \mathbb{R}_+$ is an "assimilation" (or pollution degradation) function of the environment, $D \geq 0$ is the diffusion constant, $m \geq 0$ is a coefficient, and $1 - c$ is the fraction of the economy (with output 1) assigned to pollution abatement. A simple choice for a is $a(v) = \beta v$ with $\beta > 0$, but much empirical data shows that this linear assimilation is only correct at low v, while for larger v, the "healing" capacity of the environment deterioates. Thus, following [TW96] we choose a $\kappa > 0$ and let

$$a(v) = \beta v(\kappa - v). \tag{4.2}$$

In particular, $a(v) < 0$ for $v > \kappa$, which can be thought as "runaway pollution", beyond which the pollution catalyses itself (think of global warming and permafrost thawing). Here we mostly choose this for mathematical simplicity. An alternative is to set $a(v) \equiv 0$ for $v \geq \kappa$ (no assimilation beyond the carrying capacity, but no runaway either, just "irreversible pollution"). This makes a non–differentiable at $v = \kappa$ and non–concave, which complicates matters, as discussed in [TW96, Hed09]. However, for the spatial setting the version (4.2) is interesting enough for us.

The local objective function is

$$J_c(v, c) = \ln c - \frac{\gamma}{2} v^2, \tag{4.3}$$

where $\ln c$ is the utility from consumption, and $\frac{\gamma}{2} v^2$ with $\gamma > 0$ models the costs of pollution. Pontryagin's Maximum Principle yields

$$c(\lambda) = -\frac{1}{(\delta + m)\lambda}, \tag{4.4}$$

and the canonical system reads

$$\partial_t v = -\frac{1}{\lambda} - a(v) - m + D\Delta v, \qquad v(0) = v_0, \tag{4.5a}$$

$$\partial_t \lambda = (\rho + a'(v))\lambda + \gamma v - D\Delta\lambda, \tag{4.5b}$$

with the associated 1P and 2P models as before (Δv and $\Delta\lambda$ terms dropped or replaced by discrete diffusion, respectively). We use the base parameters

$$(\delta, \beta, \kappa, \gamma, m) = (0.1, 0.01, 2, 0.01, 0.01), \tag{4.6}$$

and $\rho > 0$ as the primary bifurcation parameter.

In Fig. 4.1(a) we start with the 1P phase portrait at $\rho = 0.015$. The red dot is the unique SPP CSS $\hat{u}$, and, as before, the green line is the stable manifold $W_s(\hat{u})$, the red line the unstable manifold $W_u(\hat{u})$, the dashed lines are the nullclines, and the blue lines are selected orbits. For $0 < v_0 < \hat{v}$ we have a canonical path to $\hat{u}$, along which v and λ are monotonously increasing and decreasing, repectively, and consequently consumption starting at a high level but decreasing via

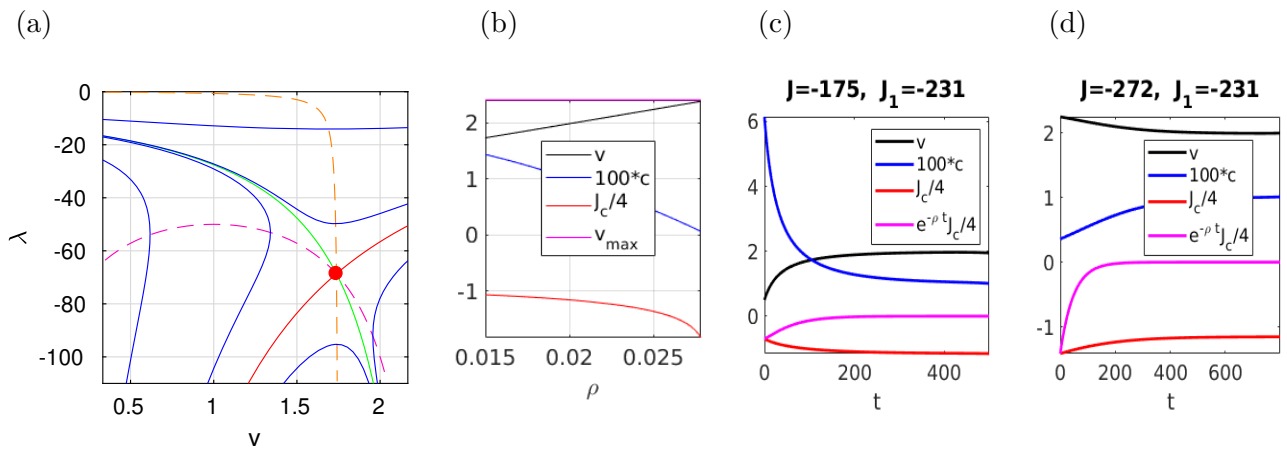

Figure 4.1: POLL 1P problem. (a) phase portrait, $\rho = 0.015$. (b) Continuation of the CSS in ρ. (c) canonical path to the CSS at $\rho = 0.02$ for $s(0) = 0.5$; high initial consumption, decreasing c and J_c, increasing s. (d) $s(0) = 2.25$, increasing c and J, decreasing s.

(4.4). However, for

$$v_0 \geq v_{\max} = \frac{\kappa}{2} + \sqrt{\frac{\kappa^2}{4} + \frac{m}{\beta}}, \tag{4.7}$$

we always have $\frac{\mathrm{d}}{\mathrm{d}t}v > -\frac{1}{\lambda} > 0$ along any canonical path. Thus, for $v > v_{\max}$ a canonical path to $\hat{u}$ does not exist. This is due to our simple choice $a(v) = \beta v(\kappa - v)$ which becomes negative for $v > \kappa$. In [TW96, Hed09], it is discussed (for a more elaborate model with $a(v) \equiv 0$ for $v \geq \kappa$) that for $v_0 > v_{\max}$ irreversible pollution paths with $\frac{\mathrm{d}}{\mathrm{d}t}v \geq 0$ and converging to another CSS $\hat{u}^*$ with $\hat{v}^* > \hat{v}$ may be optimal. Here we restrict to the simpler model (4.2), and thus for the 1P model to $v_0 < v_{\max}$. For $\hat{v} < v_0 < v_{\max}$, $\lambda(t)$ is monotonously increasing along the canonical path to $\hat{u}$, and hence also $c = -1/((\delta + m)\lambda)$ is monotonously increasing.

Figure 4.1(b) shows v, c and J_c for a continuation of the CSS in ρ, together with $v_{\max} = 1+\sqrt{2}$ for the parameter set (4.6). There exists a $\rho^* \approx 0.028$ such that $\hat{v} \nearrow v_{\max}$ and $\hat{\lambda} \to -\infty$ as $\rho \nearrow \rho^*$, and altogether the 1P model makes sense only for $0 < \rho < \rho^*$. In (c) we show the canonical path to $\hat{u}$ for small initial pollution $v(0) = 0.5$, while in (d) we let $v(0) = 2.25$. The canonical paths are as predicted by $W_s(\hat{u})$ in (a), but we remark that again the time–scale for the approach to $\hat{u}$ is rather long, and $\mathrm{e}^{-\rho t}J_c(t)$ hardly contributes to J for $t > 500$, say, since, e.g., $\mathrm{e}^{-0.015*500} \approx 5*10^{-4}$.

In Fig. 4.2 we consider the 2P problem for (4.5). The ODI criterion $h_2 > 0$ in (a, top) yields the SPP for the FCSS up to $\rho = \rho_0 \approx 0.0235$. Choosing $D = 0.01$, the blue PCSS branch $\hat{u}^{\mathrm{PCSS}}$ bifurcates at $\rho \approx 0.0238$, which yields a larger J_c than the FCSS (a, bottom), and consists of saddle points. At point 26 we have

$$\hat{u}^{\mathrm{PCSS}} = (1.503, 2.617, -116.9, -362.7), \quad c = (0.0085, 0.0027). \tag{4.8}$$

An interesting feature of the PCSSs is that at larger ρ we have $\hat{v}_j > v_{\max}$ for the patch j with the larger pollution stock (here j=2). Thus, diffusion allows one patch (one part of space) to be poisoned without runaway pollution as v may diffuse to (relatively) clean areas, where assimilation works and consumption is still relatively high. In (b) we give the value diagram of $v_{1,2}(0)$ for controlling to $\hat{u}^{\mathrm{PCSS}}$ at $\rho = 0.027$, marked by the circle. As expected, J decreases with increasing initial pollutions $v_{1,2}(0)$. For fixed truncation time $t_0 = 2000$, the numerical domain of attraction $\mathcal{A}(\hat{u}^{\mathrm{PCSS}})$ extends almost to the diagonal, and choosing larger t_0 we can obtain a somewhat larger $\mathcal{A}(\hat{u}^{\mathrm{PCSS}})$, but as already noted above, the canonical paths for $t > 500$ already hardly contribute

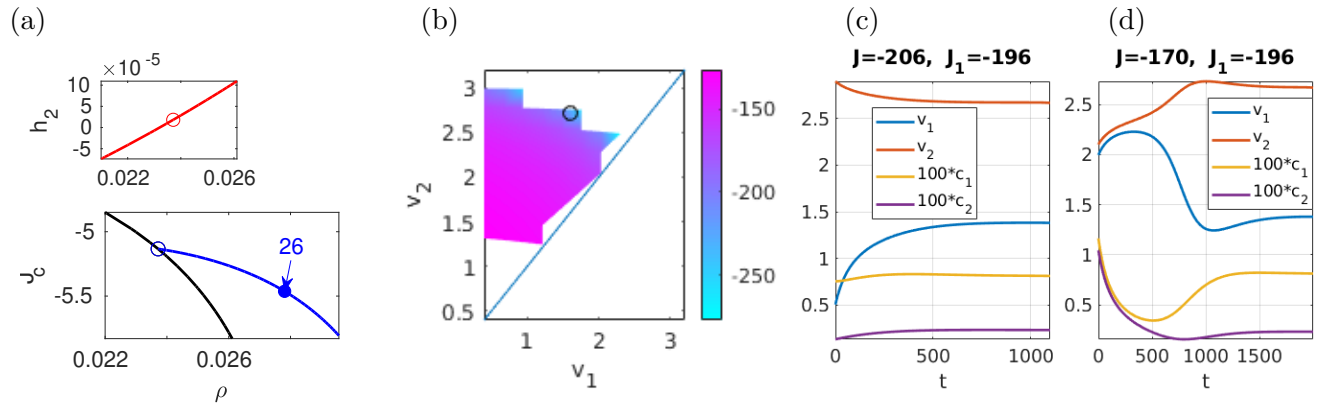

Figure 4.2: POLL, 2P, $D = 0.008$, (a) bifurcation diagram. (b) Value diagram for the PCSS $\hat{u}^{\rm PCSS}$ at $\rho = 0.027$ (marked by the circle). The domain of attraction of $\hat{u}^{\rm PCSS}$ extends almost towards the diagonal. For $v_1(0) > v_2(0)$ we get the mirror image by controlling to $M\hat{u}^{\rm PCSS}$. (c,d) two canonical paths to $\hat{u}^{\rm PCSS}$ at $\rho = 0.027$.

to the value J.

Figure 4.2(c,d) shows two such canonical paths. In (c) we have small $v_1(0) = 0.5$ and $v_2(0) = 2.9 > v_{\max}$, and the "natural" strategy is to to choose c_2 very small initially, to let $v_2(t)$ come down via diffusion; $c_1(t)$ is almost constant, and $v_1(t)$ approaches $\hat{v}_1^{\rm PCSS}$ monotonously. For large initial pollution(s) $(v_1(0), v_2(0)) = (2, 2.1)$ in (d) there is some decreasing initial consumption (also in patch 2), further increasing both pollutions. After this initial "consume what you can" phase, both $c_{1,2}(t)$ increase again to their PCSS values.

In Fig. 4.3(a,b) we present the bifurcation diagram and a sample solution for the 1D PDE case with $\Omega = (-1.5, 1.5)$, $D = 0.01$, illustrating again that in the PCSS at large ρ we can have $v > v_{\max}$ in part of the domain. For the canonical path in Fig. 1.1(c) we choose $v_0 \equiv \alpha v_{\max} + (1-\alpha)\hat{v}$ with $\alpha = 0.975$, i.e., v_0 close to $v_{\max}$ but already slightly moved towards $\hat{v}$, to reduce the time scale needed to reach the PCSS. The optimal strategy is to start with slightly smaller c on the right. This lets v initially decay there, after which consumption can increase as v is in the "optimal assimilation regime" $v{\approx}1.5$. On the other hand, the left part of the domain is "poisoned", but the diffusion is preventing runaway pollution.

In Fig. 4.3(c,d) we choose a modified v_0, namely $v_0(x){=}\hat{v}^{\rm FCSS} - x/5$, such that the left part of the domain is already initially polluted beyond the healing capacity. However, diffusion and the healing on the right again help. With small initial consumption, the assimilation lets v quickly decay on the right, after which consumption can increase as $v \approx 1.5$. The last plot in (d) shows the strongly negative shadow prices λ for this relatively large ρ. However, for slightly larger initial pollution on the left, e.g., $v_1(x){=}\hat{v}^{\rm FCSS} - x/4$, a canonical path to $\hat{u}^{\rm PCSS}$ can no longer be found. Choosing different Ω (1D or 2D), and/or different diffusion constants D, many more PCSS can be generated, but here we content ourselves with the results from Fig. 1.1(c) and Fig. 4.3.

5 Discussion

We gave examples of patterned optimal steady states (POSSs) and their canonical paths in three spatially extended infinite time horizon OC problems, FEED, FISH, and POLL. These show that POSSs occur in a variety of settings for scalar problems, in open sets in parameter space.

Our most robust example is FEED, already discussed in [UUHB21], in the sense that the POSSs have quite large domains of attraction, and going from some (homogeneous, say) initial states to a POSS yields a significant increase of the profit. This includes going from (the states

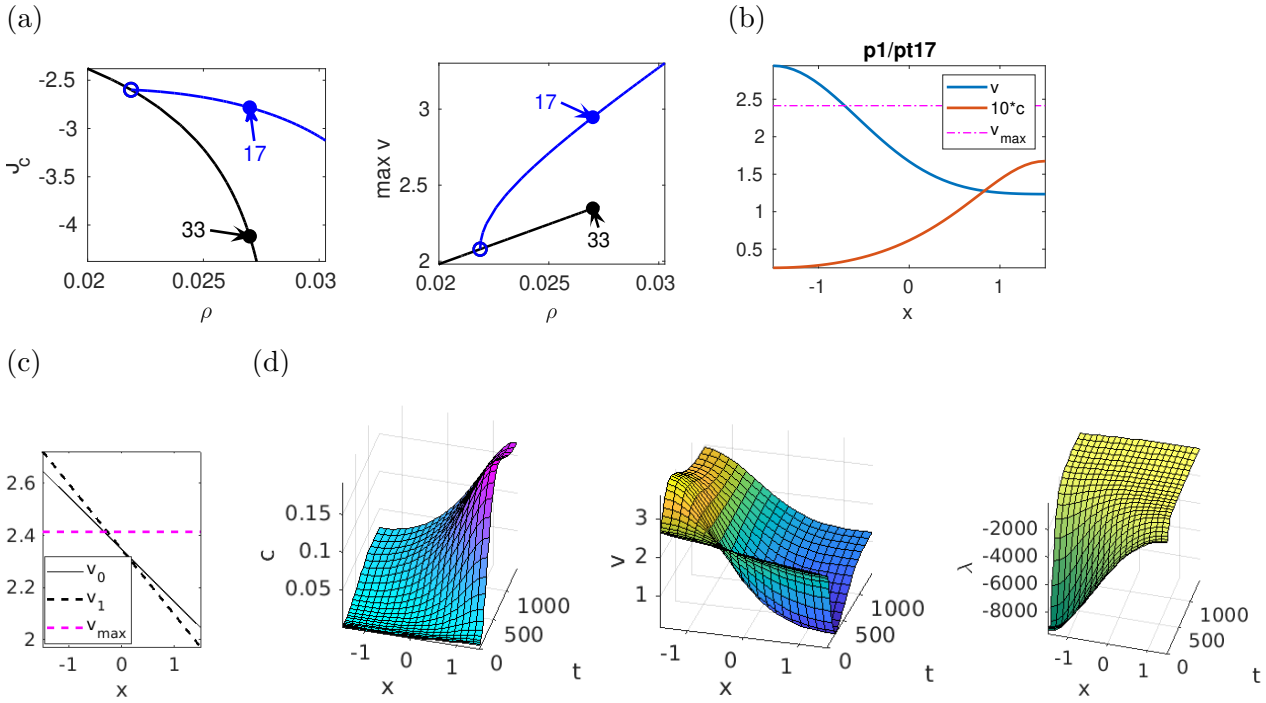

Figure 4.3: POLL, Ω=$(-1.5, 1.5)$, D=0.01. (a,b) bifurcation diagrams and a sample solution. (c) Initial states $v_0(x)$=$\hat{v}^{\mathrm{FCSS}}-x/5$ and $v_1(x)$=$\hat{v}^{\mathrm{FCSS}}-x/4$, and $v_{\max}$. For v_0, there exists a canonical path to $\hat{u}^{\mathrm{PCSS}}$ at b1/17 in (d), but not for v_1.

of) the FCSS to the POSS, and the FCSS, which may be thought as the "natural" strategy, for instance for historical reasons, is clearly not optimal.

In the FISH example we get, in large parts of parameter space, bistability of a POSS $\hat{u}^{\mathrm{PCSS}}$ with a saddle point FCSS $\hat{u}^{\mathrm{FCSS}}$, such that the values of canonical paths (if they exist) to both should be compared. However, the intersection $\mathcal{A}(\hat{u}^{\mathrm{PCSS}}) \cap \mathcal{A}(\hat{u}^{\mathrm{FCSS}})$ is rather small, and the practical applicability of our method and our results is somewhat reduced by the long transients in canonical paths which make the final convergence to the CSSs somewhat irrelevant. Nevertheless, the POSS $\hat{u}^{\mathrm{PCSS}}$ can be considered as an optimal marine reserves, and it remains to be seen if similar POSSs exist in related fishing (harvesting) models with faster convergence of canonical paths towards them.

In the POLL example, which arguably is our most simplified example and probably needs the most further modeling and parameter fitting to become "realistic", we again have POSSs with non–small domains of attraction, and probably their most striking feature is that diffusion may prevent runaway pollution: A part of the domain may be completely poisened (beyond the carrying capacity), but the pollution is balanced by diffusion of the pollution to cleaner areas, where the self–healing of the environment is still intact.

A Derivation of the CS

The canonical system (1.10) in the PDE case can be derived from the Lagrangian

$$\mathcal{L} = \int_0^\infty \mathrm{e}^{-\rho t} \left(\int_\Omega J_c(v,q) - \lambda^T (\partial_t v + G(v,q)) \, \mathrm{d}x \right) \mathrm{d}t, \tag{A.1}$$

where $G(v,q) = -f(v,q) - D\Delta v$, and where $\lambda = (\lambda_1, \ldots, \lambda_N)$ (for $N \geq 1$ components for v) can directly be identified as Lagrange multipliers to the constraint (1.10a), i.e., $\partial_t v + G(v,q) = 0$. Using integration by parts in x with the Neumann BCs $\partial_n v = 0$ and $\partial_n \lambda = 0$ we have

$$\int_\Omega \lambda^T (D\Delta v)\,\mathrm{d}x = \int_\Omega (D\Delta\lambda)^T v\,\mathrm{d}x,$$

and using integration by parts in t with the intertemporal transversality condition (1.9) yields

$$-\int_0^\infty \mathrm{e}^{-\rho t}\int_\Omega \lambda^T \partial_t v\,\mathrm{d}x\,\mathrm{d}t = \int_\Omega \lambda(x,0)^T v(x,0)\,\mathrm{d}x + \int_0^\infty \mathrm{e}^{-\rho t}\int_\Omega (\partial_t\lambda - \rho\lambda)^T v\,\mathrm{d}x\,\mathrm{d}t.$$

Thus, $\mathcal{L}$ can also be written as

$$\begin{aligned}\mathcal{L} = &\int_\Omega \lambda(x,0)^T v(x,0)\,\mathrm{d}x \\ &+ \int_0^\infty \mathrm{e}^{-\rho t}\left(\int_\Omega J_c(v,q) + (\partial_t\lambda + \rho\lambda + D\Delta\lambda)^T v + \lambda^T f(v,q)\,\mathrm{d}x\right)\mathrm{d}t,\end{aligned} \tag{A.2}$$

and (1.10a,b) are the first variations of $\mathcal{L}$ with respect to λ (using (A.1)) and v (using (A.2)) with $v(0,x)=v_0(x)$. The Hamiltonian density $H = \mathrm{e}^{-\rho t}(J_c + \lambda^T(D\Delta v + f(v,q))$ is related to the Lagrangian density $L = \mathrm{e}^{-\rho t}(J_c - \lambda^T(\partial_t v - D\Delta v - f))$ as $H = L + \mathrm{e}^{-\rho t}\lambda^T\partial_t v$, or after integration by parts in t, $H = L + \mathrm{e}^{-\rho t}(\rho\lambda - \partial_t\lambda)^T v$. Together, this yields the easy to remember general "Hamiltonian form" (1.10), i.e.,

$$\partial_t v = \partial_\lambda \widetilde{H}, \qquad \partial_t \lambda = \rho\lambda - \partial_v \widetilde{H}, \tag{A.3}$$

where $\widetilde{H}$ is the maximized Hamiltonian. As already said, both computations, i.e., the one with $\mathcal{L}$ and the one with H in [BX08], are somewhat formal, and in particular the necessity of the transversality condition (1.9) is subject to active research.

References

[BX08] W.A. Brock and A. Xepapadeas. Diffusion-induced instability and pattern formation in infinite horizon recursive optimal control. *Journal of Economic Dynamics and Control*, 32(9):2745–2787, 2008.

[BX10] W.A. Brock and A. Xepapadeas. Pattern formation, spatial externalities and regulation in coupled economic–ecological systems. *Journal of Environmental Economics and Management*, 59(2):149–164, 2010.

[Cla90] C. W. Clark. *Mathematical bioeconomics*. John Wiley & Sons, New York, second edition, 1990.

[dWU19] H. de Wit and H. Uecker. Infinite time–horizon spatially distributed optimal control problems with pde2path – algorithms and tutorial examples, arxiv:1912.11135, 2019.

[FH86] G. Feichtinger and R. Hartl. *Optimale Kontrolle ökonomischer Prozesse*. Walter der Gruyter, 1986.

[For75] B. Forster. Optimal pollution control with a nonconstant exponential rate of decay. *Environment Economics and Management*, 2:1–6, 1975.

[GCF+08] D. Grass, J.P. Caulkins, G. Feichtinger, G. Tragler, and D.A. Behrens. *Optimal Control of Nonlinear Processes: With Applications in Drugs, Corruption, and Terror*. Springer, 2008.

[GS02] M. Golubitsky and I. Stewart. *The symmetry perspective*. Birkhäuser, Basel, 2002.

[GU17] D. Grass and H. Uecker. Optimal management and spatial patterns in a distributed shallow lake model. *Electr. J. Differential Equations*, 2017(1):1–21, 2017.

[GUU19] D. Grass, H. Uecker, and T. Upmann. Optimal fishery with coastal catch. *Natural Resource Modelling*, (e12235), 2019.

[Hed09] W. Hediger. Sustainable development with stock pollution. *Environment and Development Economics*, 14:759–780, 2009.

[Hoy06] R.B. Hoyle. *Pattern formation*. Cambridge University Press., 2006.

[LW07] S. Lenhart and J. Workman. *Optimal Control Applied to Biological Models*. Chapman Hall, 2007.

[Mur89] J. D. Murray. *Mathematical biology*. Biomathematics. Springer-Verlag, Berlin, 1989.

[PBGM62] L.S. Pontryagin, V.G. Boltyanskii, R.V. Gamkrelidze, and E.F. Mishchenko. *The Mathematical Theory of Optimal Processes*. Wiley-Interscience, New York, 1962.

[Ski78] A. K. Skiba. Optimal growth with a convex-concave production function. *Econometrica*, 46(3):527–539, 1978.

[Tau15] N. Tauchnitz. The Pontryagin maximum principle for nonlinear optimal control problems with infinite horizon. *J. Optim. Theory Appl.*, 167(1):27–48, 2015.

[Tur52] A. Turing. The chemical basis of morphogenesis. *Phil. Trans. Roy. Soc. B*, 237:37–72, 1952.

[TW96] O. Tahvonen and C. Withagen. Optimality of irreversible pollution accumulation. *Journal of Economic Dynamics and Control*, 20(9-10):1775–1795, 1996.

[Uec16] H. Uecker. Optimal harvesting and spatial patterns in a semi arid vegetation system. *Natural Resource Modelling*, 29(2):229–258, 2016.

[Uec21] H. Uecker. *Numerical continuation and bifurcation in Nonlinear PDEs*. SIAM, Bookseries Mathematical Modeling and Computation, 2021. 380p, to appear.

[UUHB21] T. Upmann, H. Uecker, L. Hammann, and B. Blasius. Optimal stock enhancement activities for a spatially distributed renewable resource. *Journal of Economic Dynamics & Control*, 123:104060, 2021.

[UWR14] H. Uecker, D. Wetzel, and J.D.M. Rademacher. pde2path – a Matlab package for continuation and bifurcation in 2D elliptic systems. *NMTMA*, 7:58–106, 2014.